

Neutron Scattering from Biomaterials in Complex Sample Environments

J. Katsaras, T.A. Harroun, M.P. Nieh, M. Chakrapani, M.J. Watson,
V.A. Raghunathan

7.1 Introduction

The study of materials under difficult environmental conditions (such as high magnetic fields, high pressures, shear, and 100% relative humidity) is by no means straight forward and requires specialized equipment. These conditions may at first seem nonbiological, except for those organisms adapted to extreme environments, but a deeper understanding of biologically relevant materials has been gained from such studies.

In many cases, these experiments are made easier by the fact that neutrons interact weakly, thus nondestructively, with many commonly available materials, like aluminum and its alloys, suitable for the construction of sample cells. Their relatively low cost and useful physical characteristics mean that complex sample environments can readily be accessed with neutrons.

Lipid bilayers in water are perhaps the biologically relevant system most studied under various experimental conditions. The complex phase behavior they exhibit is of general interest to material science, as well as biology. Lipids have been subjected to extremes of temperature and pressure; have undergone detailed hydration studies; and have been aligned under shear and externally applied magnetic fields. The intrinsic properties of neutrons along with the ease of designing and constructing neutron sample environments have enabled us to probe each of these conditions.

In this chapter, we will elucidate, with a variety of recent examples, the power of neutron scattering as a tool to study biologically relevant materials in complex sample environments.

7.2 Alignment in a Magnetic Field

In order to obtain structural details on the atomic scale, the use of a single crystal sample is usually a prerequisite. However, obtaining single crystals of a desired sample is not always possible as many molecules (e.g., deoxyribose nucleic acid (DNA)) do not lend themselves to crystallization. In many such

cases, however, the use of aligned samples makes it possible to determine certain structural features of the system which can provide sufficient information to construct realistic models. Examples of aligned systems providing unique structural information are: DNA [1], plant viruses such as, tobacco mosaic virus (TMV) [2,3] and papaya mosaic virus (PMV) [4], and various lipid bilayers [5,6], to name a few.

Over the years, various strategies have been devised to orient samples that have proven either difficult or impossible to crystallize. One such strategy is to align biomolecules in an externally applied magnetic field, \mathbf{B} .

The effect of externally applied magnetic fields on biological systems has been the subject of many studies. In the 1930s, Pauling and Coryell [7] first reported the paramagnetic susceptibility of deoxyhemoglobin and the diamagnetic susceptibility of oxyhemoglobin. More recently, Higashi et al. [8] studied the orientation of erythrocytes in magnetic fields up to 8 T (tesla) and found them to orient with their disk plane parallel to \mathbf{B} . Similar behavior was observed with erythrocytes at 4 T [9].

Besides red blood cells, fibrinogen, a plasma protein, is polymerized and aligned in magnetic fields [9]. Maret et al. [10], showed that fragments of high-molecular weight native DNA partially align perpendicular to \mathbf{B} and that bases possessing diamagnetic anisotropy are responsible for this alignment. Moreover, Brandes and Kearns [11] demonstrated that liquid crystalline phases of DNA align with the long molecular axes perpendicular to \mathbf{B} . Other biological systems that have been aligned in magnetic fields are nematic phases of TMV [12] and membrane complexes such as retinal rods [13] and purple membranes of *Halobacterium halobium* [14].

With regards to living organisms, frog embryos in a 1 T field [15] exhibited no morphological differences from unexposed controls, suggesting that magnetic fields have little or no effect with normal embryonic development. However, a recent study on hemolymph samples from adult bees that had undergone pupal development and emergence in a 7 T field, contained a lower percentage of glucose than controls implying that trehalase enzyme activity is depressed in high magnetic fields [16].

7.2.1 Magnetic Alignment of Lipid Bilayers

It is generally known that lipid membranes orient with their bilayer normals perpendicular to \mathbf{B} [17] as shown in (Fig. 7.1a). This is a result of the overall negative diamagnetic anisotropy exhibited by the lipid hydrocarbon chains and their high internal order. Magnetically oriented lipid bilayered micelles, or so-called “bicelles” [18–20], possess great potential as biomimetic substrates in aligning membrane associated peptides and proteins for in-depth structural and dynamic studies. They are composed of a combination of short-chain and long-chain phosphatidylcholines (PCs) such as, dihexanoyl PC (DHPC) and dimyristoyl PC (DMPC), respectively. It is believed that the function of the

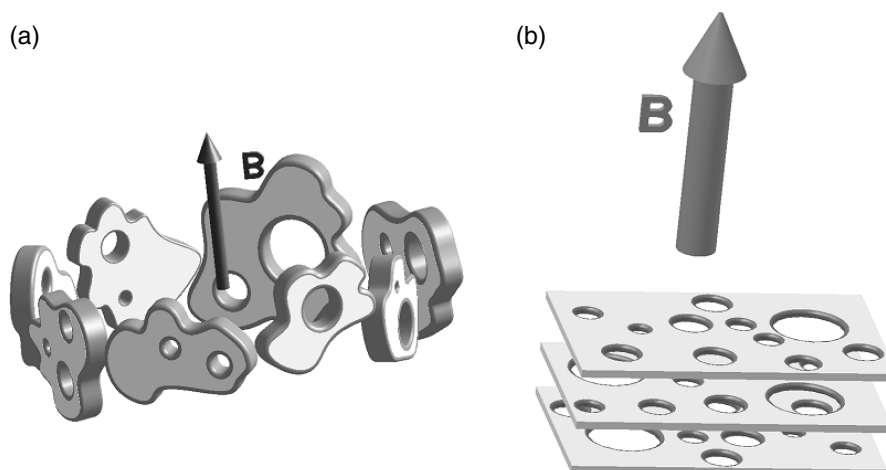


Fig. 7.1. Cartoon of (a) non-doped DMPC/DHPC mixture (DMPC:DHPC 3.2:1) in the presence of 2.6 T applied magnetic field, \mathbf{B} , and a temperature of 315 ± 1 K. Extended bilayered micelles or “finite” lamellar sheets align with their bilayer normals perpendicular to \mathbf{B} . (b) The same system as in (a) but doped with Tm^{3+} ions. In this case, the extended lamellar sheets have their bilayer normals aligned parallel to \mathbf{B} . In both the doped and nondoped cases, the bilayers are believed to be perforated [28,29]. The long-chain DMPC molecules form the bilayer while the short-chain DHPC molecules partition, primarily at the edges of the perforations and the micelles

short-chain lipid is to coat the edges of the relatively small (diameter ~ 10 – 100 nm) bilayered micelle, thus protecting the hydrophobic DMPC chains from coming into contact with water. The size of the bicelles is also dependent on the molar ratio of the two lipid species [19,21].

In a magnetic field, the orientation of DMPC/DHPC mixtures is such that the average bilayer normal, \mathbf{n} , is perpendicular to \mathbf{B} (Fig. 7.1a). In 1996, Prosser et al. [22] doped mixtures of DMPC/DHPC with paramagnetic ions, such as Tm^{3+} , and found that the orientation of the system altered such that \mathbf{n} was now parallel to \mathbf{B} (Fig. 7.1b). Compared to nondoped bicelles, the orientation of the lanthanide (e.g., Eu^{3+} , Er^{3+} , Tm^{3+} , and Yb^{3+}) doped bicelles resulted in better resolved NMR spectra. Moreover, the alignment of the nondoped bicelles restricts, due to inhomogeneous broadening of the NMR lines, the size of the membrane associated peptides that can be studied. This limitation is not there in the case of the doped bicelles [23]. Although the DMPC/DHPC bicelle mixture was reconstituted with a number of membrane-associated peptides and proteins [20,24–26], the morphology of this magnetically alignable substrate was debatable.

In a series of publications, the structures of the lanthanide-doped, DMPG-doped (dimyristoyl phosphatidylglycerol), and nondoped DMPC/DHPC systems (3.2:1, DMPC:DHPC) were reported as a function of temperature

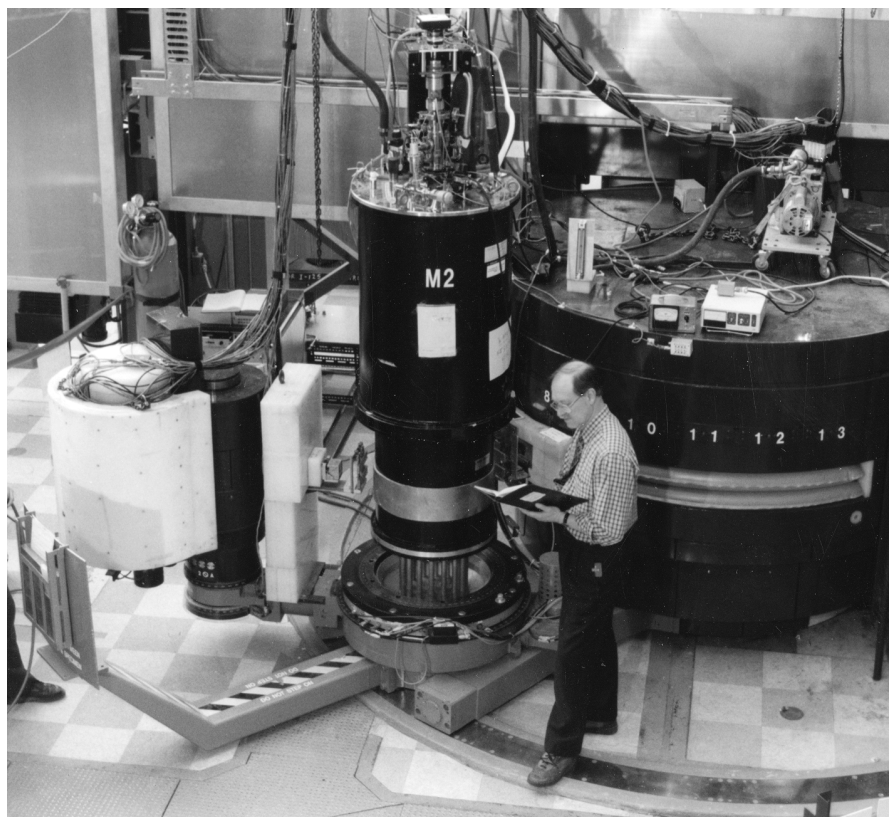


Fig. 7.2. N5 triple-axis spectrometer with M2 superconducting magnet/cryostat located at the NRU reactor (Chalk River, Canada). 2.37 Å wavelength neutrons were selected using the (002) reflection of a pyrolytic graphite monochromator. The M2 magnet/cryostat is a somewhat unique instrument in that it produces a horizontal, rather than a vertical magnetic field

and total lipid concentration [27–29]. Using the C5 and N5 triple-axis spectrometers (Fig. 7.2) located at the National Research Universal (NRU) reactor (Chalk River, Canada) and 2.37 Å neutrons, the samples were subjected to a 2.6 T horizontal magnetic field (Fig. 7.2), as in the NMR experiment.

At a temperature of 315 ± 1 K, the nondoped DMPC/DHPC mixture suspended in 77 wt% D_2O formed a nematic phase, characterized by a single broad peak centered at $Q \sim 0.05 \text{ \AA}^{-1}$ ($Q = 2\pi/d$, where d is the lamellar repeat spacing) (Fig. 7.3a), and resulting from bilayered micelles or small bilayer sheets possessing long-range orientational order but lacking positional order [27]. In this phase, the system's bilayer normals are perpendicular to the magnetic field (Fig. 7.1a) and analogous to a lipid/detergent system studied by X-ray scattering [30]. Upon addition of Tm^{3+} ions (DMPC: Tm^{3+} , 7.5:1), the system underwent a nematic \rightarrow smectic transition, as exemplified by the

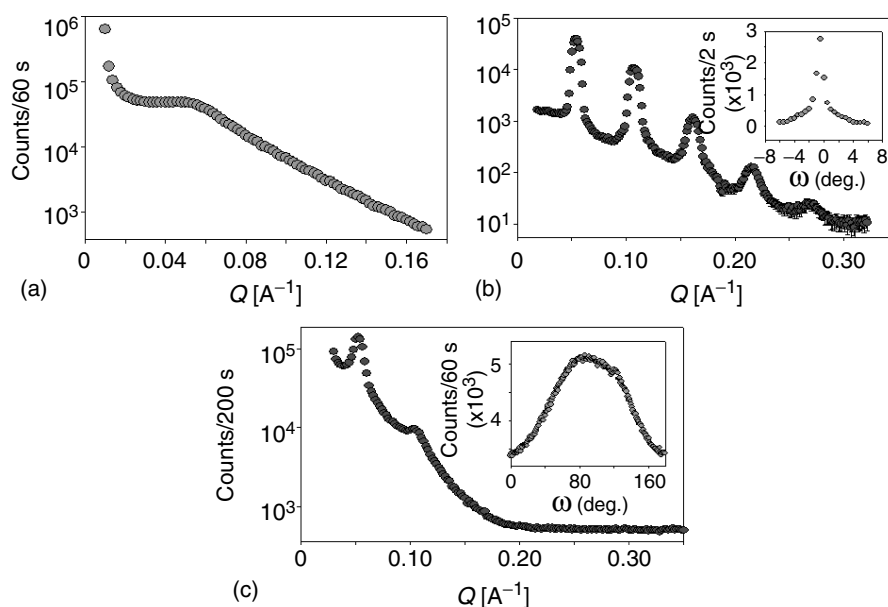


Fig. 7.3. Scan in Q of (a) DMPC/DHPC system in the absence of Tm^{3+} , at a T of 315 K and a 2.6 T field. The broad peak centered at $\sim 0.05 \text{ \AA}^{-1}$ is indicative of a nematic phase (1D ordering, see Fig. 7.1). (b) The addition of Tm^{3+} ions results in a smectic phase (2D order) with well-defined Bragg reflections. The inset to the figure shows that the phase is highly aligned, within a degree, or so, of the applied magnetic field. (c) Removal of the magnetic field results in a less ordered smectic phase, as indicated by the rocking curve (inset), with the lamellar spacing remaining unaltered. For further details the reader is referred to [27]

appearance of well-defined Bragg reflections (Fig. 7.3b), and indicative of a system possessing a well-defined interbilayer spacing, d , of 116 Å. Moreover, the system was shown to be highly aligned with the rocking curve having an FWHM of $\leq 1^\circ$ (inset to Fig. 7.3b). In the absence of an applied magnetic field, the orientation of the system is, for the most part, lost (Fig. 7.3c and inset) while the phase remained unaltered. In summary, the doping of the DMPC/DHPC mixture with Tm^{3+} ions resulted in the system undergoing a nematic \rightarrow smectic transition while the magnetic field imparted an alignment to the system [27]. The above-mentioned study was later refined, in the absence of a magnetic field, using small-angle neutron scattering (SANS) [28, 29] and whose partial phase diagrams are presented below (Fig. 7.4).

7.2.2 Neutron Scattering in a Magnetic Field: Other Examples

In 1989, Hayter et al. [31], reported on SANS measurements of ferrofluids containing TMV and tobacco rattle virus (TRV). In this case, the nonmagnetic

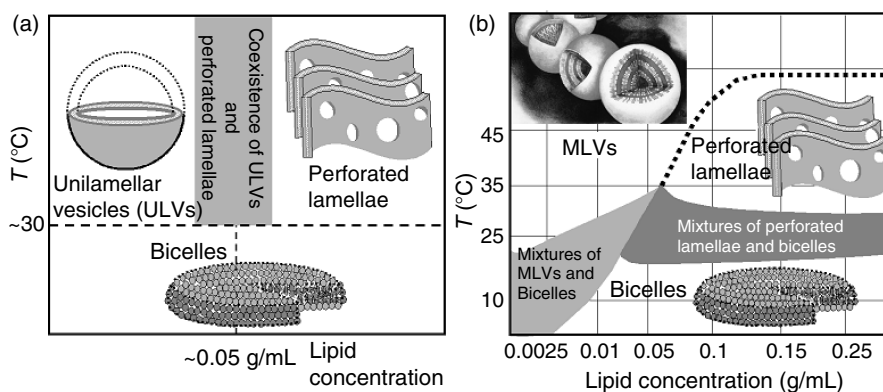


Fig. 7.4. Partial phase diagrams of (a) the Tm^{3+} -doped DMPC/DHPC system at a ratio of 3.2:1 (DMPC:DHPC) and (b) the non-doped DMPC/DHPC system. In the Tm^{3+} -doped system two morphologies are observed at high temperatures (T): Unilamellar vesicles (ULVs) at lipid concentrations approximately 0.01 g ml^{-1} and perforated lamellae at concentrations 0.05 g ml^{-1} wt%. For T below 15°C , the mixture exhibits an isotropic phase composed of bilayered micelles. Compared to Tm^{3+} -doped DMPC/DHPC mixtures, the nondoped DMPC/DHPC system exhibits a much more complex phase behaviour, and the appearance of multilamellar vesicles (MLVs) instead of ULVs seen previously in the Tm^{3+} -doped system. The SANS data used to determine the various morphologies were collected at the National Institute of Standards and Technology (NIST, Gaithersburg, USA) using the NG-7 30 m instrument

viruses were aligned by the magnetic ferrofluid in a modest external field. Using this colloidal dispersion the contrast between the dispersed particles and the ferrofluid carrier was altered giving rise to information with regards to some structural features of these systems. Since most biological materials possess neither sufficiently anisotropic magnetic properties to align in a magnetic field nor morphological characteristics to respond to alignment *via* shear, ferro-dispersed suspensions offer a method of aligning colloidal particles in suspension. In addition, their ability to align in low concentrations is particularly important when it comes to samples which are not readily available in large quantities.

Groot et al. [32] reported on SANS studies carried out using Na-DNA fragments at concentrations between 190 and 285 mg ml^{-1} . Applying a magnetic field either perpendicular or parallel to the incident neutron beam they were able to deduce the cholesteric or chiral nematic structure of the liquid crystalline solutions. When \mathbf{B} was applied in a direction parallel to the incident neutron beam the small-angle scattering was found to be isotropic. This is not surprising as the incident beam was parallel to the pitch of the cholesteric phase. On the other hand, when the direction of \mathbf{B} was changed to be perpendicular to the incident neutron beam, the resultant scattering was

anisotropic. It should be noted that the average direction of DNA molecules is perpendicular to the magnetic field.

Kiselev et al. [33], determined the orientation of pure DMPC MLVs below and close to the main gel–liquid crystalline transition, T_M , and of DMPC/ $C_{12}E_8$ (dodecyl-octaethyleneoxide) mixed micelles in magnetic fields from 1 to 4 T. It was determined that spherical DMPC vesicles deform to an ellipsoidal shape at $\mathbf{B} = 2$ T while the mixed micelles of DMPC/ $C_{12}E_8$ forms a Gaussian-coil, composed of rod-like micelles, irrespective of the magnetic field strength. In the case of liquid crystalline DMPC vesicles, the degree of deformation was more pronounced than gel phase DMPC vesicles.

Mucins are polyelectrolytes whose rigidity can be altered as a function of pH. For stomach mucins, molecular weights of between 2×10^5 and 1.6×10^7 Da have been reported with their structure related to the function that they perform, namely to protect the stomach epithelium from its surrounding environment. They supposedly do so by forming dense viscoelastic gels at low pH (e.g., pH 2) [101] and the side chain interdigitation is crucial in the network’s formation [102]. A recent study by Waigh et al. [103] showed that in the absence of a magnetic field these side chains form a polydomain nematic phase, while a monodomain phase is induced when a 1.48 T magnetic field is applied. The magnetic field was found to orient the molecules with their long axis pointing in the direction of the field. Moreover, the field was used to study the nature of entanglement couplings between the side chains.

7.3 High Pressure Studies

The potential of pressure in biological systems as a thermodynamic variable remains largely unexplored even though pressures experienced by many aquatic organisms is in the range of ~ 50 MPa, or greater. At these pressures, there are most likely, significant effects on macromolecular structure and function.

Pressure has the effect of reversibly denaturing proteins and can therefore be used as a means of studying protein folding and protein interactions [34,35]. In the recent past, high pressure has emerged as a method to stabilize folding intermediates [34]. The molecular basis of protein–RNA and protein–DNA recognition is intricately related to the thermodynamics of the system. Recent studies have shown that pressure can inactivate viruses while preserving their immunogenic properties [36,37].

One of the least developed areas using pressure is high-pressure protein crystallography. Kundrot and Richards [38] carried out the first high pressure X-ray crystallographic study using hen egg-white lysozyme at a pressure of 100 MPa using a dead end-bored beryllium rod [39]. A similar device was used to study sperm whale myoglobin at 150 MPa [40]. More importantly, Urayama et al. [40] developed a technique whereby the pressurized crystal is cooled, “freezing-in” pressure-induced collective movements and eliminating a pressure cell during data collection. Studies on myoglobin [41,42],

lysozyme [39, 43, 44] and staphylococcal nuclease [45] show that protein crystals are robust and can withstand substantial amounts of pressure.

An area of ongoing interest is the effect of hydrostatic pressure on lipid phase behavior and dynamics. The response of lipid bilayers to pressure can provide some insight into the effect of other perturbations at ambient pressure. Pressure dependent structure and phase behavior of lipid systems has been studied over the years by Winter and co-workers using a combination of X-ray and neutron scattering [46–49].

7.3.1 Hydrostatic Pressure and Aligned Lipid Bilayers

The main gel–liquid crystalline transition (T_M) in lipid bilayers has attracted a great deal of attention in the last few decades. In the case of phosphatidylcholine lipids such as DMPC, one outstanding issue is with regards to the structural changes occurring in the vicinity of the main transition. On decreasing temperature, the lamellar repeat spacing, d , of liquid crystalline DMPC bilayers increases nonlinearly. This nonlinear increase in lamellar repeat spacing, or “anomalous swelling,” in the vicinity of T_M , has previously been reported by various groups studying PC bilayers [50–59]. The commonly accepted view is that this anomalous swelling is a pretransitional effect.

One possibility, put forth by Nagle in 1973, is that a critical transition gets intercepted by the first-order main transition [60]. Another point of view is that due to some intrinsic bilayer property, the main transition itself is weakly first-order [61]. Recently, Pabst et al. [62] demonstrated that the majority of the anomalous swelling is the result of increasing interbilayer water, and a sudden decrease of the bilayer bending rigidity, K_c . Of importance is that the functional form of K_c follows a power law dependence near T_M .

In 1986, Lipowsky and Leibler [63] predicted the critical unbinding (i.e., loss of periodicity) of a membrane stack, due to steric repulsion, independent of the anomalous swelling phenomenon occurring in lipid bilayers. One reason that leads to membranes unbinding, is a reduction in K_c causing bilayers to undulate and repel each other [63]. It therefore seems that one can relate thermal unbinding and anomalous swelling, both the result of a decrease in K_c , leading to a temperature dependence of the lamellar periodicity, given by $d \approx (T - T_c)^{-\psi}$, where T_c is the unbinding temperature. The critical exponent, ψ , is predicted to be unity.

If the functional form of K_c with respect to temperature is reflected in the functional form of the anomalous swelling, then pressure can be used to interrogate the region in the vicinity of T_M . Pressure also allows one to study the behavior of short chain lipids whose T_M is below 0°C.

Compared to isotropic or “powder” samples the use of aligned samples is highly desirable as the signal from these samples is anisotropic and usually easier to decipher. In the case of X-ray or neutron scattering an oriented sample

allows for the differentiation of the inter-bilayer (lamellar repeat spacing) and intra-bilayer (hydrocarbon chain correlations) organization [64]. Also, due to the fact that the signal is not spread-out over 2π , much less sample is required to obtain a good signal to noise ratio.

Watson et al. [65] recently constructed a sample cell suitable for neutron scattering from aligned lipid multibilayers and capable of exerting hydrostatic pressures up to 370 MPa over a temperature range of between -10 and 100°C (Fig. 7.5a). The advantage of this cell compared to other high-pressure neutron cells [66, 67] is that it allows for the study of samples whose quantities are limited and in conjunction with a 2D detector the in-plane and out-of-plane correlations can easily be obtained both as a function of temperature and pressure.

Aluminum was chosen as the material to construct the cell as it is practically transparent to neutrons. At ambient temperatures Al is reasonably corrosion resistant. However, the same cannot be said at elevated temperatures. In order to retard the corrosion process the sample block was hard anodized (Fig. 7.5b). Although the measures taken did reduce the amount of

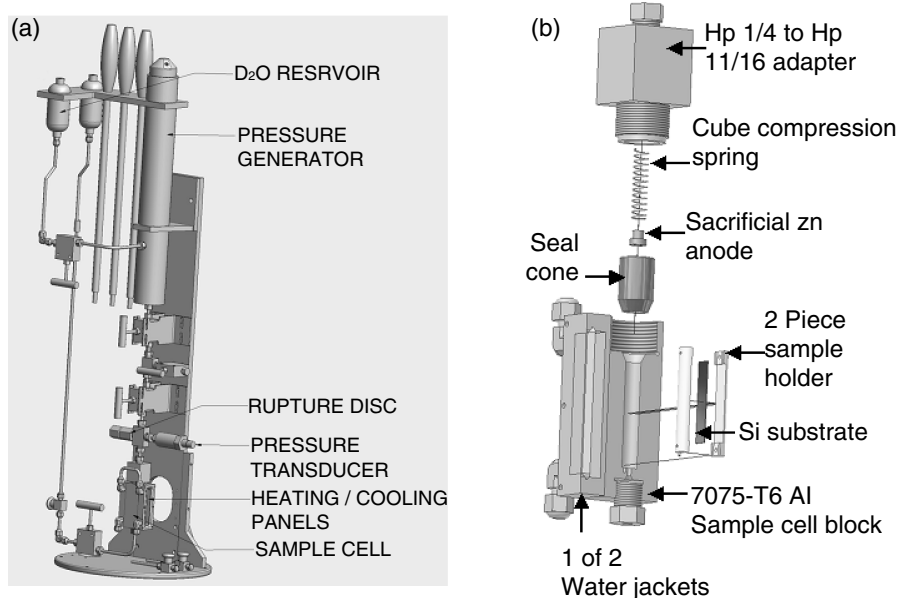


Fig. 7.5. (a) Pressurized sample cell assembly rated for hydrostatic pressures up to 370 MPa and suitable for neutron diffraction of aligned biomimetic systems. (b) Neutron sample cell assembly constructed from 7075-T6 Al alloy. The sample cell was hard anodized to reduce corrosion and fitted with helicoils, on both ends, to reduce stretching of the threads. A Zn sacrificial anode was used to further retard the corrosion process much evident at elevated temperatures. For further details please refer to [65]

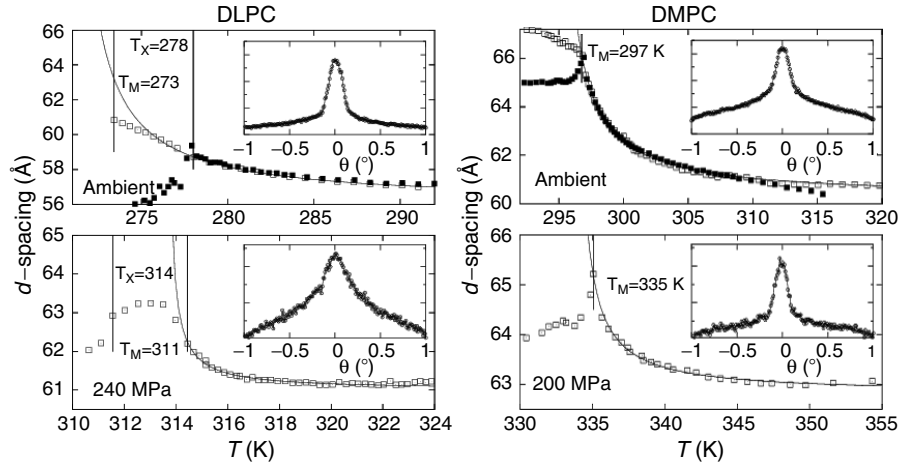


Fig. 7.6. Lamellar repeat spacings, d , as a function of temperature and a given hydrostatic pressure for fully hydrated dilauroyl phosphatidylcholine (DLPC) and DMPC multibilayer stacks. The insets to the figures depict so-called “rocking curves,” a direct measure of the samples alignment. The open and closed symbols were obtained upon cooling and heating, respectively. The solid lines are the best fits to the equation $d - d_0 \propto (T - T^*)^{-\psi}$. For further details please see [65, 68]

corrosion, nevertheless the maximum attainable temperature at 370 MPa of hydrostatic pressure, was $\leq 60^\circ\text{C}$.

Figure 7.6 shows the relationship between d and T at a given pressure for dilauroyl phosphatidylcholine (DLPC) and DMPC aligned multibilayers [68]. The data were fitted to the power law form proposed by Lemmich et al. [53] namely $d - d_0 \propto (T - T^*)^{-\psi}$ where d_0 is the repeat spacing well into the liquid crystalline phase (high T), and ψ , the critical exponent, is 1. It was interesting to note that as a function of increasing pressure there is a definite decrease in the amount of anomalous swelling taking place in DMPC bilayers and that the power law form of anomalous swelling is preserved up to 240 MPa of hydrostatic pressure. The anomalous swelling of DMPC bilayers is found to decrease with increasing pressure, but the functional form of K_c near T_M is preserved even at the highest pressure used.

An important result from these studies was that in DLPC bilayers complete unbinding may take place at hydrostatic pressures in excess of 290 MPa [68]. Presently, we have been unable to carry-out the requisite experiments to test this prediction as our sample cell has proven, due to corrosion, incapable of attaining the necessary hydrostatic pressures. However, we are in the process of designing and constructing a new cell made out of copper/beryllium.

7.3.2 High Pressure Neutron Scattering Experiments: Other Examples

Czeslik et al. [46] studied the lateral organization of the binary lipid mixture, DMPC/DSPC (distearoyl phosphatidylcholine) at hydrostatic pressures up to 100 MPa. What was observed was an increase of 22°C/100 MPa of applied pressure of the two phase coexistence region. They also noted the existence of fractal-like membrane morphologies within the gel–liquid crystalline coexistence region and not the kind of phase separation that one would anticipate on the basis of the thermodynamic equilibrium phase diagram. Compared to ambient pressure, the fractal exponent of coexistence mixture changed slightly at 100 MPa.

Worcester and Hammouda [69] studied, as a function of temperature and pressure, the behavior of PC lipids with C20 (diarachidoyl, DAPC) and C22 (dibehenoyl, DBPC) hydrocarbon chains. Worcester and Hammouda observed that DBPC formed interdigitated bilayers at pressures <60 MPa while DAPC formed a similar phase at 60 MPa of pressure showing that the minimum pressure for interdigitation changes systematically with the length of the hydrocarbon chains. Other disaturated PCs, such as DPPC and DSPC (distearoyl phosphatidylcholine) have also been observed to form such interdigitated phases [70].

Doster and Gebhardt [71] reported on the dynamics and stability of myoglobin. As a function of pressure, the evolution of the protein–solvent bonds and the unfolding transition were observed. The pressure-induced unfolding of the protein took place above 300 MPa with ≈40% of the protein’s helical structures being preserved in the unfolded state. Doster and Gebhardt concluded that pressure enhanced protein–solvent interactions may be a factor in destabilizing the native state of the protein.

Loupiac et al. [72] reported on horse azidometmyoglobin (MbN₃) at pressure up to 300 MPa. As a function of pressure the protein’s radius of gyration remained unaltered up to 300 MPa. From the second virial coefficient of the protein solution the authors determined that the protein–protein repulsive forces, although diminished, were never overcome even at 300 MPa while the specific volume of MbN₃, compared to atmospheric pressure, decreased by 5.4% at 300 MPa.

Köhling et al. [73] studied the phase behavior of dioctyl sulfosuccinate sodium (AOT)-*n*-octane–water mesophases as a function of pressure (0.01–300 MPa). The incorporation of the water-soluble enzyme α-chymotrypsin with the surfactant mixtures resulted in significant changes to the structure and phase behavior of the various surfactant mesophases with the observed changes enhanced with increasing pressure. The application of pressure resulted in fluid lamellar and bicontinuous surfactant phases. Ultimately, the changes in α-chymotrypsin activity, as a function of pressure, were attributed to changes in the surfactant mesophase structure and not to any changes in tertiary or secondary protein structure.

AQ: [64] has been changed to [71] according to reference list. ok!

7.4 Shear Flow Induced Structures in Biologically Relevant Materials

Some of the earliest reports of the use of shear flow to study soft materials were by Scheraga and Backus [74], and Ackerson and Clark [75]. Since then, the use of shear has allowed the observation of shear-induced structural transformations in a wide variety of soft materials [76]. Shear-induced transformations in complex fluids include: micellar elongation and alignment [77], isotropic to nematic transitions [78] and the formation of multilamellar vesicles [79–81]. In the case of biologically relevant materials shear has been used to crystallize various fats (e.g., milk fat, cocoa butter) [82], study the aggregation of casein micelles in undiluted skim milk [83], measure the extent and rate of adhesion of leukemia cells [84], and the alignment of lecithin reverse micelles [85], to name a few. In all of the above-mentioned studies, shearing devices of different geometries have been developed to induce the necessary shear.

7.4.1 Shear Cells Suitable for Neutron Scattering

Over the years, a variety of shear cells have been developed for the study of shear-induced structures using X-ray [86–90] and neutron [91–98] scattering techniques. Shear gradients $>10^3 \text{ s}^{-1}$ needed to study colloidal particles and micellar solutions are readily achievable by either Poiseuille or Couette type cells (Fig. 7.7). Generally, Couette flow is preferable because the cell diameter (d) is much smaller than the gap width (r) resulting in a constant gradient across the gap, whereas the characteristic flow in a Poiseuille cell has a parabolic velocity profile [99].

The first widely used Couette type cell suitable for neutron scattering was constructed by Lindner and Oberthur at the Institut Laue-Langevin (ILL). In the Couette geometry the sample is sheared between two concentric cylinders, usually made out of polished quartz. The inner cylinder, the stator, is stationary while the outer one rotates (rotor). The difference in velocity between the outer and inner cylinders divided by the gap separating them, gives rise to the average applied shear experienced by the sample. Although the basic Couette design has remained relatively unaltered since its inception, nevertheless in the last couple of years improvements to the basic design have been made. One such improvement has been made by Porcar et al. [98], whereby they have designed a cell capable of operating at shear rates up to $15,000 \text{ s}^{-1}$ without liquid losses due to evaporation. The cell, like many others of its type, is temperature controlled and capable of accepting sample volumes as low as 7 ml.

A shear cell suitable for the study of liquid–solid interfaces by neutron reflectometry and SANS was designed a decade ago by Baker et al. [94]. The shear rates were altered by changing, over three orders of magnitude, the volume flow through the cell under laminar flow conditions. Recently, a new type of shear cell designed for the study of interfaces was described by Kuhl

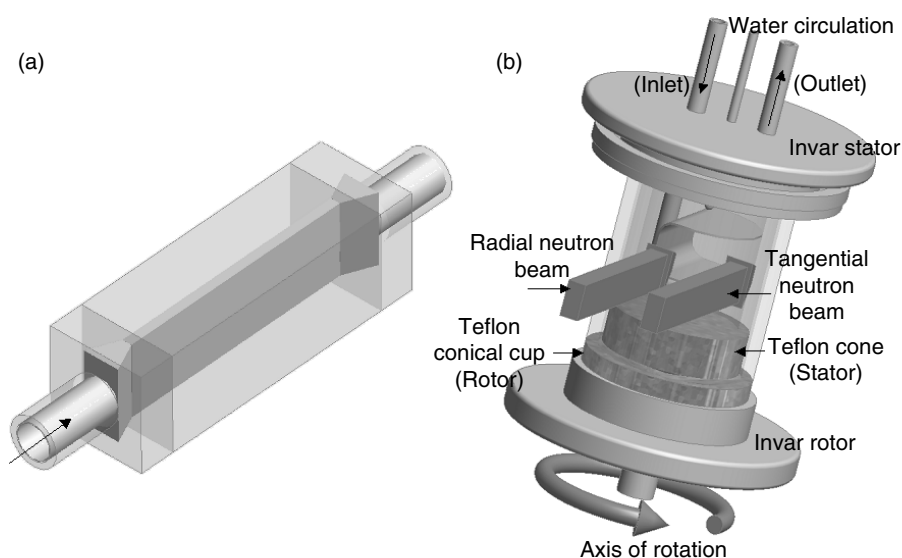


Fig. 7.7. (a) Poiseuille flow cell made out of quartz. (b) A typical concentric cylinder Couette type shear cell. Couette flow results in a constant gradient across the gap, whereas the characteristic in a Poiseuille cell is that shear rate tends to zero toward the center of the flow cell. Both the Poiseuille and Couette type shear cells are capable of being interrogated in the radial and tangential directions. For further information the reader is referred to [95] and [98]

et al. [97]. This shear cell, suitable for neutron reflectometry, has the ability to control surface separation (i.e., gap) and alignment under applied loads. The gap size is variable from millimeters to <100 nm and capable of exerting steady shear rates from 0.001 to 20 s^{-1} . The difference between the two above-mentioned reflectometry shear cells is that the one by Kuhl et al. [97] achieves shear by the lateral motion of the lower substrate relative to the stationary upper substrate. Throughout the shearing process the substrates maintain a defined gap separation. The difference between the Baker et al. [94] and Kuhl et al. [97] shear cells is that for the latter case, the shear is occurring at the substrate interface rather than the solvent flow/sample interface as in the case of the cell by Baker et al.

7.4.2 Shear Studies of Biologically Relevant Systems

Shear cells have traditionally been used to examine polymeric systems, however, over the years there have been examples of studies investigating biologically relevant materials. Schurtenberger et al. [85] studied the alignment of

lecithin/isooctane solutions using a Couette type shear cell and SANS. They obtained, as a function of shear rate, direct evidence of water-induced cylindrical (anisotropic) growth in reverse micelles in a 1 mm gap. The amount of sample required was only 8 ml.

Renard et al. [100] studied the effect of shear on the structure of a protein-polysaccharide mixture, namely bovine serum albumin (BSA)/hydroxyethyl cellulose (HEC) or BSA/carboxymethyl cellulose (CMC). SANS measurements carried out under static and shear conditions (0.5 mm gap and shear rates between 0.1 and 100 s^{-1}) indicated that shear aligned the various mixtures, with some preferential alignment taking place along the direction of flow. This anisotropy, however, disappeared at elevated shear rates.

There is a growing interest in hierarchical molecular self-assembly as such nanostructured materials may have commercial potential. For example, certain peptides exhibit a variety of supramolecular structures as a function of increased peptide concentration in water [104]. Recently, Mawer et al. [105] studied the possible mesoscopic structures responsible for the nonlinear rheology of self assembling peptide fibrils and fibrillar networks. As a function of shear rate ($0\text{--}500 \text{ s}^{-1}$), the orientation of the nematic director in the fluid and gel phases was studied using SANS. In the velocity direction (radial), self assembled fibril structures consisted of 8–10 single β -sheet tapes (single molecule thick) which upon gelation increased to between 10 and 12 tapes. At moderate shear rates, SANS data was found to be consistent with that of an oriented nematic gel network formed of semiflexible fibrils, while at high shear rates the linkages between the fibrils broke leading to a reduction in sample viscosity.

7.5 Comparison of a Neutron and X-ray Sample Environment

Under any circumstance, the study of materials in difficult environments is not trivial. However, because of their penetrating power (interact weakly) with many commonly available materials, particularly aluminum and its alloys, neutrons have a distinct advantage over X-rays in construction simplicity and cost. Besides aluminum, other commonly used materials for sample cell environments are vanadium and $\text{Ti}_{66}\text{:Zr}_{34}$ commonly used as a null scattering alloy. As mentioned previously, Cu–Be alloy and Maraging steel are suitable for high pressure studies, while for high temperatures sapphire and Inconel have been used [106]. All of these materials have almost no transparency to X-rays. Here we present an example of a neutron and X-ray sample cell capable of fully hydrating aligned lipid multibilayer stacks.

7.5.1 100% Relative Humidity Sample Cells

In elucidating structure, there are advantages of studying aligned lipid multibilayer stacks as opposed to isotropic multilamellar vesicles. The problem was

that when the lipid bilayers aligned on a solid support were hydrated in a 100% relative humidity (RH) environment, the lamellar repeat spacing, d , was found to be consistently smaller than the same MLV material immersed in bulk water [107–109]. This posed a serious problem as in equilibrium, the chemical potential of water vapor at 100% RH and that of bulk water, are the same. Since these results are paradoxical, this discrepancy between samples hydrated from 100% RH and bulk water came to be known as the vapor pressure paradox (VPP) [110]. Moreover, in 1997 a theory was published to explain the underlying mechanism of VPP [111].

The theory by Podgornik and Parsegian [111] stated that lipid bilayers aligned on rigid supports experience a global suppression of bilayer fluctuations, not just at the sample interfaces, as a result of the rigid substrate and the lipid/water vapour interface. This reduction in bilayer fluctuations results in smaller entropic repulsion pressures and concomitantly, reduced d . A somewhat less elegant explanation was that all of the data contributing to the VPP were obtained from experiments utilizing sample cells that were incapable of attaining 100% RH.

To elucidate this discrepancy between theory and experiment, a sample environment suitable for neutron diffraction was designed with the following characteristics: (a) Reduce temperature gradients. (b) Minimize the volume around the sample. (c) Have an “evaporative surface” in close proximity to the sample. A sample cell, similar to the one in Fig. 7.8a, was designed and built at Chalk River Laboratories (Canada). The neutron diffraction results conclusively demonstrated that VPP was an artifact due to poorly designed sample cells over a period of three decades [112].

The concepts of the 100% RH neutron cell (Fig. 7.8a) were transferred to a sample cell suitable for X-ray diffraction (Fig. 7.8b) [64]. Comparing the two cells (Fig. 7.8), one can easily come to the conclusion that the X-ray cell is a much more complicated device. This was necessary as X-rays are generally not highly penetrating and require special, nonabsorbing “window” materials. These windows possess different thermal properties than the other materials used in constructing the sample cell, leading to the possibility of thermal gradients and the reality of RHs <100%. Nevertheless, the X-ray sample cell, shown in Fig. 7.8b, was able to achieve the requisite humidities and yielded results indistinguishable from those obtained from neutrons scattering experiments. However, the costs of design, construction, and implementation of the X-ray cell were ≈ 20 times that of the neutron sample environment.

7.6 Conclusions

It is the hope of the authors that this brief review has provided the reader with comprehensive information to the various sample environments, suitable for biologically relevant studies, and presently used by the various neutron scattering laboratories worldwide. It should be said that there are few, if

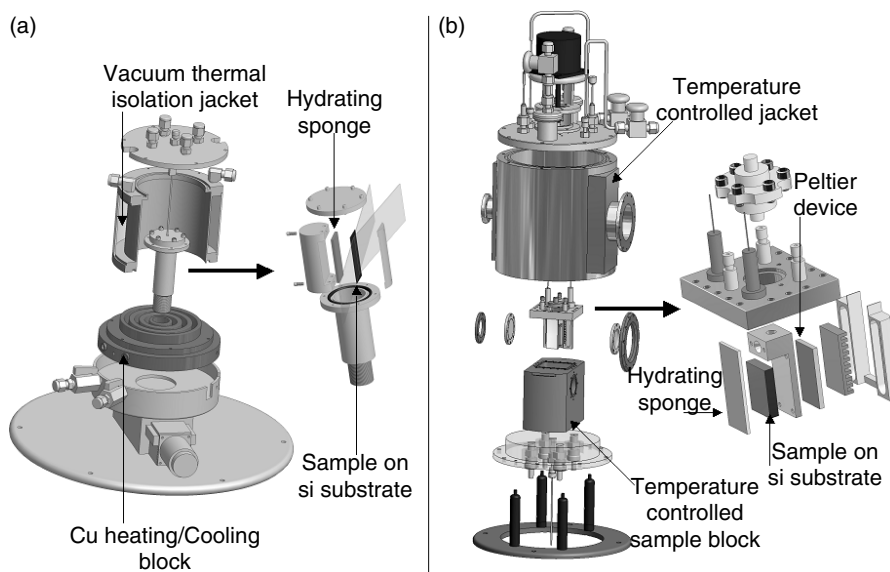


Fig. 7.8. Comparison of (a) 100% relative humidity (RH) cell suitable for neutron scattering and (b) similar cell suitable for X-ray diffraction. Because X-rays are easily absorbed, choosing the materials to construct various parts of the sample cell is not trivial and results, in comparison to the neutron sample cell, in a rather complicated design with concomitant costs. Moreover, and unlike the X-ray sample cell, the one for suitable neutrons can be filled with liquid water. For further information with regards to these two samples environments the reader is referred to [64, 112, 113]

any, sample environments that exist for neutron scattering that cannot be replicated for use with X-rays. Generally speaking, however, because the interaction of neutrons with many commonly used materials is weak, the design of a particular sample environment, compared to the one for use with X-rays, is simplified.

Up to now there have not been an abundance of biologically relevant studies that have used the sample environments described in the present review. However, the hope is that the benefits presently experienced by the colloidal and polymer communities will become evident to those studying biomimetic materials especially, the use of shear to align systems as shear cells are ubiquitous in neutron scattering laboratories.

The use of hydrostatic pressure is another potential growth area as the interest in protein unfolding is ever increasing. Future samples cells capable of routinely exerting 500–600 MPa of hydrostatic pressure are not out of the question.

References

1. J.D. Watson, F.H.C. Crick, *Nature* **171**, 737 (1953)
2. J.D. Bernal, I. Fankuchen, *J. Ge. Physiol.* **28**, 111 (1941)

3. J. Gregory, K.C. Holmes, *J. Mol. Biol.* **13**, 796 (1965)
4. P. Tollin, J.B. Bancroft, J.F. Richardson, N.C. Payne, T.J. Beveridge, *Virology* **98**, 108 (1979)
5. J. Katsaras, V.A. Raghunathan, *Phys. Rev. Lett.* **74**, 2022 (1995)
6. V.A. Raghunathan, J. Katsaras: *Phys. Rev. Lett.* **74**, 4456 (1995)
7. L. Pauling, C. Coryell, *Proc. Natl. Acad. Sci. U.S.A.* **22**, 210 (1936)
8. T. Higashi, A. Yamagishi, T. Takeuchi, N. Kawaguchi, S. Sagawa, S. Onishi, M. Date, *Blood* **82**, 1328 (1993)
9. A. Yamagishi, *J. Mag. Mag. Mat.* **90**, 43 (1990)
10. G. Maret, M. V. Schickfus, A. Mayer, K. Dransfeld, *Phys. Rev. Lett.* **35**, 397 (1975)
11. R. Brandes, D. Kearns, *Biochemistry* **25**, 5890 (1986)
12. X. Ao, X. When, R.B. Meyer, *Physica A* **176**, 63 (1991)
13. M. Chabre, *Proc. Natl. Acad. Sci. USA* **75**, 5471 (1978)
14. B. Lewis, L.C. Rosenblatt, R.G. Griffin, J. Courtemanche, *Biophys. J.* **47**, 143 (1985)
15. S. Ueno, K. Harada, K. Shiokawa, *IEEE Trans. Magn.* **MAG-20**, 1663 (1984)
16. J. Kefuss, K. M'Diaye, M. Bounias, J. Vanpoucke, J. Ecochard, *Bioelectromagnetics* **20**, 117 (1999)
17. G. Maret, K. Dransfeld, D.M. MacKay, Strong and ultrastrong magnetic fields and their applications, in: *Topics in Applied Physics*, vol. 57, ed. by, F. Herlach (Springer, New York, 1985), pp. 143–204
18. P. Ram, J.H. Prestegard, *Biochim. Biophys. Acta* **940**, 289 (1988)
19. C.R. Sanders, J.P. Schwonek, *Biochemistry* **31**, 8898 (1992)
20. C.R. Sanders, B.J. Hare, K.P. Howard, J.H. Prestegard, *Prog. NMR Spectrosc.* **26**, 421 (1994)
21. R.R. Vold, R.S. Prosser, *J. Magn. Reson. B* **113**, 267 (1996)
22. R.S. Prosser, S.A. Hunt, J.A. DiNatale, R.R. Vold, *J. Am. Chem. Soc.* **118**, 269 (1996)
23. R.S. Prosser, V.B. Volkov, I.V. Shiyanovskaya, *Biophys. J.* **75**, 2163 (1998)
24. C.R. Sanders, G.C. Landis, *Biochemistry* **34**, 4030 (1995)
25. G.C. Sanders, R.S. Prosser, *Ways & Means* **6**, 1227 (1998)
26. J. Struppe, E.A. Komives, S.S. Taylor, R.R. Vold, *Biochemistry* **37**, 15523 (1998)
27. J. Katsaras, R.L. Donaberger, I.P. Swainson, D.C. Tennant, Z. Tun, R. R. Vold, R. S. Prosser, *Phys. Rev. Lett.* **78**, 899 (1997)
28. M.-P. Nieh, C.J. Glinka, S. Krueger, R.S. Prosser, J. Katsaras, *Langmuir* **17**, 2629 (2001)
29. M.-P. Nieh, C.J. Glinka, S. Krueger, R.S. Prosser, J. Katsaras, *Biophys. J.* **82**, 2487 (2002)
30. B.J. Hare, J.H. Prestegard, D.M. Engleman, *Biophys. J.* **69**, 1891 (1995)
31. J.B. Hayter, R. Pynn, S. Charles, A.T. Skjeltorp, J. Trehwella, G. Stubbs, P. Timmins, *Phys. Rev. Lett.* **62**, 1667 (1989)
32. L.C.A. Groot, M.E. Kuil, J.C. Leyte, J.R.C. van der Maarel, *Liq. Cryst.* **17**, 263 (1994)
33. M.A. Kiselev, M. Janich, P. Lesieur, A. Hoell, J. Oberdisse, G. Pepy, A.M. Kisselev, L.V. Gapienko, T. Gutberlet, V. L. Aksenov, *Appl. Phys. A [Suppl.]* **74**, S1239 (2002)
34. J.L. Silva, D. Foguel, C.A. Royer, *Trends Biochem. Sci.* **26**, 612 (2001)
35. C. Balny, P. Masson, K. Heremans, *Biochim. Biophys. Acta* **1595**, 3 (2002)

36. L.P. Gaspar, A.C. Silva, A.M. Gomes, A.P.D. Ano Bom, W.D. Schwarcz, J. Mestecky, M.J. Novak, D. Foguel, J.L. Silva, *J. Biol. Chem.* **277**, 8433 (2002)
37. A.M.O. Gomes, A.S. Pinheiro, C.F.S. Bonafe, J.L. Silva, *Biochemistry* **42**, 5540 (2003)
38. C.E. Kundrot, F.M. Richards, *J. Mol. Biol.* **193**, 157 (1987)
39. C.E. Kundrot, F.M. Richards, *J. Appl. Cryst.* **19**, 208 (1986)
40. P. Urayama, G.N. Phillips Jr., S.M. Gruner, *Structure* **10**, 51 (2002)
41. U.F. Thomanek, F. Parak, R.L. Mössbauer, H. Formanek, P. Scwager, W. Hoppe, *Acta Crystallogr.* **A29**, 263 (1973)
42. R.F. Tilton Jr., G.A. Petsko, *Biochemistry* **27**, 6574 (1988)
43. A. Katrusiak, Z. Dauter, *Acta Crystallogr.* **D52**, 607 (1996)
44. R. Fourme, R. Kahn, M. Mezouar, E. Girard, C. Hoerentrup, T. Prangè, I. Ascone, *J. Synchrotron Radiat.* **8**, 1149 (2001)
45. F. Österberg, Induced changes in the diffuse X-ray scattering background from protein crystals. PhD Thesis (Princeton University, New Jersey, 1996)
46. C. Czeslik, J. Erbes, R. Winter, *Europhys. Lett.* **37**, 577 (1997)
47. R. Winter, J. Erbes, C. Czeslik, A. Gabke, *J. Phys.: Condens. Matter* **10**, 11499 (1998)
48. R. Winter, C. Czeslik, *Z. Kristallogr.* **215**, 454 (2000)
49. R. Winter, *Biochim. Biophys. Acta* **1595**, 160 (2002)
50. S. Kirchner, G. Cevc, *Europhys. Lett.* **23**, 229 (1993)
51. T. Hønger, K. Mortensen, J.H. Ipsen, J. Lemmich, R. Bauer, O.G. Mouritsen, *Phys. Rev. Lett.* **72**, 3911 (1994)
52. R. Zhang, W. Sun, S. Tristram-Nagle, R.L. Headrick, R.M. Suter, J.F. Nagle, *Phys. Rev. Lett.* **74**, 2832 (1995)
53. J. Lemmich, K. Mortensen, J.H. Ipsen, T. Hønger, R. Bauer, O.G. Mouritsen, *Phys. Rev. Lett.* **75**, 3958 (1995)
54. F.Y. Chen, W.C. Hung, H.W. Huang, *Phys. Rev. Lett.* **79**, 4026 (1997)
55. J.F. Nagle, H.I. Petrache, N. Gouliev, S. Tristram-Nagle, Y. Liu, R.M. Suter, K. Gawrisch, *Phys. Rev. E* **58**, 7769 (1998)
56. F. Richter, L. Finegold, G. Rapp, *Phys. Rev. E* **59**, 3483 (1999)
57. S.S. Korreman, D. Posselt, *Eur. Phys. J.* **1**, 87 (2000)
58. P.C. Mason, J.F. Nagle, R.M. Epand, J. Katsaras, *Phys. Rev. E* **63**, 030902 (2001)
59. S.S. Korreman, D. Posselt, *Eur. Biophys. J.* **30**, 121 (2001)
60. J.F. Nagle, *Proc. Natl. Acad. Sci. USA* **70**, 3443 (1973)
61. D.P. Kharakoz, E.A. Shlyapnikova, *Phys. Chem. B* **104**, 10368, (2000)
62. G. Pabst, J. Katsaras, V. Raghunathan, M. Rappolt, *Langmuir* **19**, 1716 (2003)
63. R. Lipowsky, S. Leibler, *Phys. Rev. Lett.* **56**, 2541 (1986)
64. J. Katsaras, M.J. Watson, *Rev. Sci. Instrum.* **71**, 1737 (2000)
65. M.J. Watson, M.-P. Nieh, T.A. Harroun, J. Katsaras, *Rev. Sci. Instrum.* **74**, 2778 (2003)
66. R. Winter, W.-C. Pilgrim, *Ber. Bunsenges. Phys. Chem.* **93**, 708 (1989)
67. G.W. Neilson, D.I. Page, W.S. Howells, *J. Phys. D* **12**, 901 (1979)
68. T.A. Harroun, M.-P. Nieh, M.J. Watson, V.A. Raghunathan, G. Pabst, M.R. Morrow, J. Katsaras; *Phys. Rev. E* **69**, 031906 (2004)
69. D. Worcester, B. Hammouda, *Physica B* **241–243**, 1175 (1998)
70. L.F. Braganza, D.L. Worcester, *Biochemistry* **25**, 2591 (1986)
71. W. Doster, R. Gebhardt, *Chem. Phys.* **292**, 383 (2003)

AQ: Please update
Ref. [68]

72. C. Loupiac, M. Bonetti, S. Pin, P. Calmettes, *Eur. J. Biochem.* **269**, 4731 (2002)
73. R. Köhling, J. Woenckhaus, N.L. Klyachko, R. Winter, *Langmuir* **18**, 8626 (2002)
74. H.A. Scheraga, J.K. Backus, *J. Am. Chem. Soc.* **73**, 5108 (1981)
75. B.J. Ackerson, N.A. Clark, *Phys. Rev. A* **30**, 906 (1984)
76. P.D. Butler, *Curr. Opin. Colloid Interface Sci.* **4**, 214 (1999)
77. P.D. Butler, L.J. Magid, W.A. Hamilton, J.B. Hayter, B. Hammouda, P.J. Kreke, *J. Phys. Chem.* **100**, 443 (1996)
78. E. Cappelaere, J.F. Berret, J.P. Decruppe, R. Cressely, P. Lindner, *Phys. Rev. E* **56**, 1869 (1997)
79. O. Diat, D. Roux, F. Nallet, *J. Phys. II* **3**, 1427 (1993)
80. J. Zipfel, P. Lindner, M. Tsianou, P. Alexandridis, W. Richtering, *Langmuir* **15**, 2599 (1999)
81. J. Zipfel, J. Berghausen, P. Lindner, P. Richtering, *J. Phys. Chem. B* **103**, 2841 (1999)
82. G. Mazzanti, S.E. Guthrie, E.B. Sirota, A.G. Marangoni, S.H.J. Idziak, *Cryst. Growth Des.* **3**, 721 (2003)
83. D. Lehner, P. Worning, G. Fritz, L. Øgøndal, R. Bauer, O. Glatter, *J. Colloid Interface Sci.* **213**, 445 (1999)
84. D.G. Swift, R.G. Posner, D.A. Hammer, *Biophys. J.* **75**, 2597 (1998)
85. P. Schurtenberger, L.J. Magid, J. Penfold, R. Heenan, *Langmuir* **6**, 1800 (1990)
86. R.J. Plano, C.R. Safinya, E.B. Sirota, L.J. Wenzel, *Rev. Sci. Instrum.* **64**, 1309 (1993)
87. J.A. Pople, I.W. Hamley, G.P. Diakun, *Rev. Sci. Instrum.* **69**, 3015 (1998)
88. Ch. Münch, J. Kalus, *Rev. Sci. Instrum.* **70**, 187 (1999)
89. P. Baroni, C. Pujolle-Robic, L. Noirez, *Rev. Sci. Instrum.* **72**, 2686 (2001)
90. M. Ksilak, H. Anderson, N.S. Babcock, M.R. Stetzer, S.H.J. Idziak, E.B. Sirota, *Rev. Sci. Instrum.* **72**, 4305 (2001)
91. P. Lindner, R.C. Oberthur, *Rev. Phys. Appl.* **19**, 759 (1984)
92. G.C. Straty, H.J.M. Hanley, C.J. Glinka, *J. Stat. Phys.* **62**, 1015 (1991)
93. L. Kalus, G. Neubauer, U. Schmelzer, *Rev. Sci. Instrum.* **61**, 3384 (1990)
94. S.M. Baker, G. Smith, R. Pynn, P. Butler, J. Hayter, W. Hamilton, *Rev. Sci. Instrum.* **65**, 412 (1994)
95. V.M. Cloke, J.S. Higgins, C.L. Phoon, S.M. Richardson, S.M. King, R. Done, T.E. Cooper, *Rev. Sci. Instrum.* **67**, 3158 (1996)
96. G.C. Straty, C.D. Muzny, P.D. Butler, M.Y. Lin, T.M. Slawecki, C.J. Glinka, H.J.M. Hanley, *Nucl. Instrum. Methods Phys. Res. A* **408**, 511 (1998)
97. T.L. Kuhl, G.S. Smith, J.N. Israelachvili, J. Majewski, W. Hamilton, *Rev. Sci. Instrum.* **72**, 1715 (2001)
98. L. Porcar, W.A. Hamilton, P.D. Butler, G.G. Warr, *Rev. Sci. Instrum.* **73**, 2345 (2002)
99. P.G. Cummins, E. Staples, B. Millen, J. Penfold, *Meas. Sci. Technol.* **1**, 179 (1990)
100. D. Renard, F. Boué, J. Lefebvre, *Physica B* **234–236**, 289 (1997)
101. X. Cao, R. Bansil, K.R. Bhaskar, B.S. Turner, T.J. LaMont T. Niu, N.H. Afdhal, *Biophys. J.* **76**, 1250 (1999)
102. L.A. Sellers, A. Allen, E.R. Morris, S.B. Ross-Murphy, *Carbohydr. Res.* **178**, 93 (1988)
103. T.A. Waigh, A. Papagiannopoulos, A. Voice, R. Bansil, A.P. Unwin, C.D. Dewhurst, B. Turner, N. Afdhal, *Langmuir* **18**, 7188 (2002)

104. A. Aggeli, I.A. Nyrkova, M. Bell, R. Harding, L. Carrick, T.C.B. McLeish, A. N. Semenov, N. Boden, *Proc. Natl. Acad. Sci. USA* **98**, 11857 (2001)
105. P.J. Mawer, T.A. Waigh, R. Harding, T.C.B. McLeish, S.M. King, M. Bell, N. Boden, *Langmuir* **19**, 4940 (2003)
106. I.F. Bailey, *Z. Kristallogr.* **218**, 84 (2003)
107. J. Torbet, M.H.F. Wilkins, *J. Theor. Biol.* **62**, 447 (1976)
108. N.P. Franks, W.R. Lieb, *J. Mol. Biol.* **133**, 469 (1979)
109. J. Katsaras, *J. Phys. Chem.* **99**, 4141 (1995)
110. R.P. Rand, V.A. Parsegian, *Biochim. Biophys. Acta* **988**, 351 (1989)
111. R. Podgornik, V.A. Parsegian, *Biophys. J.* **72**, 942 (1997)
112. J. Katsaras, *Biophys. J.* **75**, 2157 (1998)
113. G. Pabst, J. Katsaras, V. A. Raghunathan, *Phys. Rev. Lett.* **88**, 128101 (2002)